Measurement report: Analysis of aerosol optical depth variation at Zhongshan Station in Antarctica

Lijing Chen[1,2], Lei Zhang[1], Yong She[2], Zhaoliang Zeng[1], Yu Zheng[1], Biao Tian[1], Wenqian Zhang[1], Zhaohui Liu[3], Huizheng Che[*1], Minghu Ding[*1]

[1] State Key Laboratory of Severe Weather, Chinese Academy of Meteorological Sciences, Beijing, 100081, China.

[2] Chengdu University of Information Technology, Chengdu, 610103, China.

[3] Polar Surveying and Mapping Engineering Center of Heilongjiang Administration of Surveying, Mapping and Geoinformation,Harbin 150081, China

Correspondence to: Minghu Ding (dingminghu@foxmail.com), Huizheng Che (chehz@cma.gov.cn)

Three key findings:

- The AOD level over Zhongshan Station in Antarctica is low in summer and high in winter. AE indicates the dominance of fine (coarse) aerosols in summer (winter).

- In winter and spring, high AOD values are related to the increase of coarse mode particles, while in summer and autumn, high AOD values may be related to the growth of fine mode particles.

- AOD varied inversely with wind speed and showed an insignificant positive correlation with temperature but a significant negative correlation with relative humidity.

Abstract: Our understanding of aerosol optical depth (AOD) in Antarctica remains limited due to the scarcity of ground observation stations and limited daylight days. Utilizing data from the CE318-T photometer spanning from January 2020 to April 2023 at Zhongshan Station, we analysed the seasonal, monthly, and diurnal variations in AOD and Ångström exponent (AE). AOD median values increased from spring (0.033) to winter (0.115), while AE peaked during summer (1.010) and autumn (1.034), declining in winter (0.381), indicating a transition in dominant aerosol particle size from fine to coarse mode between summer and winter. Monthly mean AOD variation closely paralleled the proportion of AE<1, suggesting fluctuations in coarse mode particle proportions drive AOD variation. The high AOD values during winter and spring were associated with increased contribution of coarse mode particles, while high AOD values during summer and autumn were associated with the growth of fine mode particles. We observed a peak in AOD (~0.06) at 14:00 local time at Zhongshan Station, possibly

associated with a slight decrease in boundary layer height (BLH). Additionally, higher (lower) wind speeds corresponded to lower (higher) AOD values, indicating the diffusion (accumulation) effect. The temperature and AOD showed an insignificant positive correlation ($R = 0.22$, $p = 0.40$), relative humidity exhibited a significant negative correlation with AOD ($R = -0.59$, $p = 0.02$). Backward trajectory analysis revealed that coarse particles from the ocean predominantly contributed to high AOD daily mean values, while fine particles on low AOD days originated mainly from the air mass over the Antarctic Plateau. This study enhances the understanding of the optical properties and seasonal behaviors of aerosols in the coastal Antarctic. Specifically, AOD measurements during the polar night address the lack of validation data for winter AOD simulations. Additionally, we revealed that lower wind speeds, higher temperatures, and lower relative humidity contribute to increased AOD at Zhongshan Station, and air masses from the ocean significantly impact local AOD levels. These findings help us infer AOD variation patterns in the coastal Antarctic based on meteorological changes, providing valuable insights for climate modeling in the context of global climate change.

1 Introduction

Aerosols play an important role in impacting the climate system by absorbing and scattering solar radiation (Li et al., 2022). Antarctica, considered one of the most pristine lands, serves as an ideal background area for evaluating the climate effects of aerosols (Kamra, 2022). Marine aerosols emitted from the Southern Ocean are a primary source contributing to the aerosol load in Antarctica (Thakur, 2019). The retreat of sea ice in Antarctica is expected to escalate the release of sea salt and secondary biogenic aerosols (Yan et al., 2020). Sea salt particles with strong scattering may produce negative effective radiative forcing or indirect radiative effect by influencing cloud condensation nuclei within the marine boundary layer over Antarctica (Thornhill et al., 2021; Udisti et al., 2012). However, the heating effect of absorbent aerosols, such as black carbon (BC), may be amplified by the high surface albedo in Antarctica (Kang et al., 2020). In recent years, there has been a notable increase in BC concentrations in Antarctica, with BC deposition on snow and ice surfaces contributing to reduced surface albedo and increased solar radiation absorption, subsequently accelerating snow and ice melt (Kannemadugu et al., 2023). Given the close connection between aerosol radiation effects and their

57 optical properties (Che et al., 2024), it is necessary to investigate the optical parameters of Antarctica

58 aerosols.

59 Aerosol optical depth (AOD), as a key parameters of aerosol optical properties, serves as an effective

60 measure of aerosol load and can influence the solar radiation components (Alghoul et al., 2009). AOD

61 observation records from Antarctica sites indicate that the values range from 0.006 to 0.220 in coastal

62 regions and from 0.007 to 0.034 in inland regions (Kannemadugu et al., 2023; Tomasi et al., 2007, 2012;

63 Yang et al., 2021). Typically, coastal aerosols consist primarily of coarse-mode sea salt particles during

64 austral winter, while fine-mode particles (such as dimethyl sulfide and its oxidation product mesylate,

65 DMS, and MSA) lead to elevated particle number concentrations in summer (20-100 times higher than

66 in winter) (Lachlan-Cope et al., 2020; Shaw, 1979). Conversely, aerosols over the Antarctic Plateau

67 predominantly comprise fine-mode particles of non-sea-salt sulfate (NSS) and DMS (Harder et al., 2000;

68 Walters et al., 2019).

69 Additionally, particle size plays a significant role in aerosol extinction. The Ångström exponent (AE)

70 serves as an important indicator of aerosol size, with value greater (less) than 1 indicating a predominance

71 of fine (coarse) mode particles (Schuster et al., 2006). Weller and Lampert report that the mean AE at

72 Neumayer Station was 1.5 ± 0.6 and 1.2 ± 0.5 during summer and winter, respectively, suggesting an

73 increased contribution of fine-mode biological sulfate particles in summer (Weller and Lampert, 2008).

74 Virkkula et al. observed higher scattering AE estimate values during summer (~1.9) and lower values

75 during winter (~0.8) at Dome C on the Antarctic Plateau, indicating a prevalence of fine particles in

76 summer (Virkkula et al., 2022).

77 Currently, the challenging environment and the limited number of daylight days per year restrict the

78 availability of ground sites capable of obtaining adequate AOD and AE observations. Consequently, the

79 optical properties of aerosols across large parts of Antarctica remain unexplored. To improve our

80 comprehension of aerosol properties in Antarctica, we analyse the seasonal, monthly, and diurnal

81 variations of AOD and AE using data obtained from the recently installed sun-sky-lunar CE318-T

82 photometer at Zhongshan Station.

2 Site, Instrument, and Data

2.1 Site Introduction

Zhongshan Station (69°22′12″S, 76°21′49″E, 18 m a.s.l.) is located at the Larsemann Hills of Prydz Bay on the east Antarctic continent. The sun-sky-lunar CE318-T photometer is installed at Swan Ridge, northwest of the Nella fjord (Fig. 1) (Tian et al., 2022). This location experiences 54 polar days and 58 polar nights annually, with snow covering the surrounding surface during winter and revealing bare rock in summer. In this study, the austral spring, summer, autumn, and winter are referred to the season from September to November (SON), December to February of next year (DJF), March to May (MAM), and June to August (JJA), respectively. The average annual air temperature is -10 ℃, with a relative humidity of 58% and prevailing wind speeds of 6.9 $m\,s^{-1}$, primarily from the east or east-southeast direction (Ding et al., 2022).
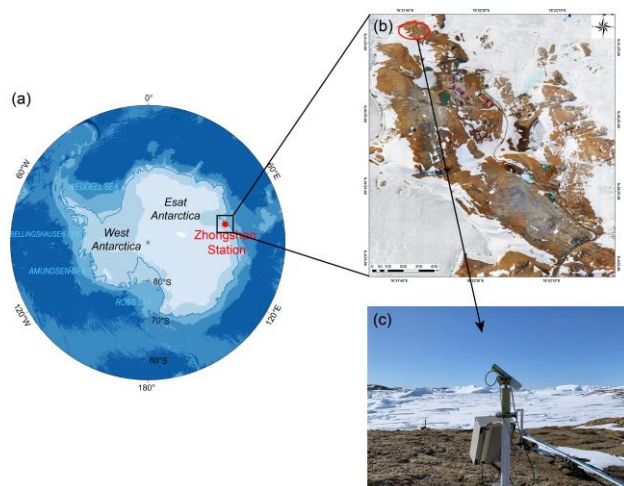
Figure 1 (a) The location of Zhongshan Station in Antarctica, (b) the aerial view of Zhongshan Station, and (c) the sun-sky-lunar photometer CE318-T at Zhongshan Station.

2.2 Instrument and Data

The AOD measurement data utilized in this study were obtained from the sun-sky-lunar CE318-T photometer, manufactured by CIMEL Electronique, France. The CE318-T is a ground-based multiband radiometer capable of inverting aerosol optical parameters by measuring the spectral data of direct solar and lunar radiation extinction and the angular distribution of sky radiances (Barreto et al., 2016).

102 We collected AOD level 1.5 (cloud-screened) data across various wavelengths spanning from January

103 2020 to April 2023 (Fig. S1). However, the operation of CE318-T in polar environment is impeded by

104 solar radiation and weather conditions, leading to a significant number of missing measurements.

105 Consequently, we categorize daily observations with less than 20 measurements and the coefficient of

106 dispersion (CV) exceeding 1 as invalid data, which are systematically eliminated from our analysis.

107 Typically, these invalid data manifest with exceedingly high AOD values, often attributed to instrument

108 downtime caused by factors such as precipitation or cloudy weather. Moreover, to ensure the accuracy

109 of AOD measurement at Zhongshan Station, we refine our data by cross-referencing station operation

110 records and the time series of black carbon (BC) concentrations. This process allows us to exclude AOD

111 data associated with significant station activities and periods of elevated BC concentrations, thereby

112 enhancing the reliability of our analysis. It should be noted that there are uncertainties in the AOD

113 measurements of CE318-T during field observations due to atmospheric conditions, instrument noise,

114 and calibration. It is estimated that during daytime measurements, the AOD uncertainty ranges from

115 0.010 to 0.021. For night-time measurements, the AOD uncertainty depends on the calibration technique

116 used. Specifically, when calibrated using the Moon Ratio technique, the uncertainty ranges from 0.011

117 to 0.019. With the application of the new Sun Ratio technique, the uncertainty for the 440 nm channel is

118 between 0.012 and 0.015 (0.017), while for longer wavelengths, it ranges from 0.015 to 0.021. By

119 employing the new Sun-Moon gain factor technique and using the Langley-calibrated instrument for

120 calculation of the amplification between daytime and night-time measurements, the uncertainty range is

121 from 0.016 to 0.019 (Barreto et al., 2016).

122 The meteorology data, including temperature, relative humidity, wind direction, and wind speed, were

123 obtained from the Zhongshan Station meteorology observatory, with the temporal resolution of 1 hour.

124 BLH data was obtained from ERA5 reanalysis provided by European Centre for Medium Range Weather

125 Forecasts (ECMWF) with the temporal and spatial resolution of 1 hour and 0.25 (latitude) × 0.25

126 (longitude).

127 The Hybrid Single-Particle Lagrangian Integrated Trajectory (HYSPLIT) model, is a comprehensive

128 model developed by the National Oceanic and Atmospheric Administration (NOAA) and the Air

129 Resources Laboratory (ARL) to calculate and analyse the source, transport, and diffusion trajectories of

130 atmospheric pollutants. The meteorological data used in the HYSPLIT model comes from the National

131 Center for Environmental Prediction (NCEP) Global Data Assimilation System (GDAS). In this study,

132 the HYSPLIT model is utilized to calculate the 168h backward air mass trajectory from 3 altitudes of 50,

133 500, and 1000 m (amsl) to Zhongshan Station.

134 **3 Results**

135 **3.1 Variation Characteristics of AOD**

136 From January 2020 to March 2023, the monthly mean AOD values at various wavelengths varied from

137 0.00 to 0.20, with the lowest values in December 2020 and the highest values in August 2022 (Fig. 2a).

138 The monthly mean AOD values at 500 nm ($AOD_{500\,nm}$) generally remained below 0.10, consistent with

139 findings by Gadhavi and Achuthan at the Maitri Station, where AOD variation fell within the range of

140 0.01 to 0.10 (Gadhavi and Achuthan, 2004). The annual mean $\pm$ SD (standard deviation) values of the

141 $AOD_{500\,nm}$ were 0.074$\pm$0.090, 0.051$\pm$0.066, 0.071$\pm$0.117, and 0.053$\pm$0.031 in 2020, 2021, 2022, and

142 2023, respectively (Table 1). Similarly, the annual mean $\pm$ SD values of the $AE_{440\text{-}870\,nm}$ were

143 1.134$\pm$0.411, 0.953$\pm$0.338, 0.883$\pm$0.374, 0.753$\pm$0.206 for the same years, respectively, suggesting that

144 the aerosols over Zhongshan Station were mainly dominated by fine mode particles in 2020, and coarse

145 mode particles in 2021, 2022, and 2023. The relationship between multi-year $AOD_{500\,nm}$ and $AE_{440\text{-}870\,nm}$

146 illustrates that fine mode particles are primarily concentrated in the range of $AOD_{500\,nm} < 0.1$, while high

147 $AOD_{500\,nm}$ values, which occur occasionally, are caused by coarse mode particles (Fig. 2b). Although

148 fine mode particles have a longer suspension time in the atmosphere and can efficiently scatter and absorb

149 sunlight, leading to lower AOD ranges, it is worth mentioning that in the coastal regions of Antarctica,

150 the dominant role in AOD is sometimes played by coarse mode particles. These particles, with larger

151 radii and higher volume concentrations, originate mainly from abundant sea salt sources. Their presence

152 results in increased scattering and absorption of sunlight, emphasizing the significance of coarse mode

153 particles in determining AOD levels in the Antarctic coastal areas (Su et al., 2022)

删除了: Table 1

设置了格式: 字体: 10 磅, 非加粗
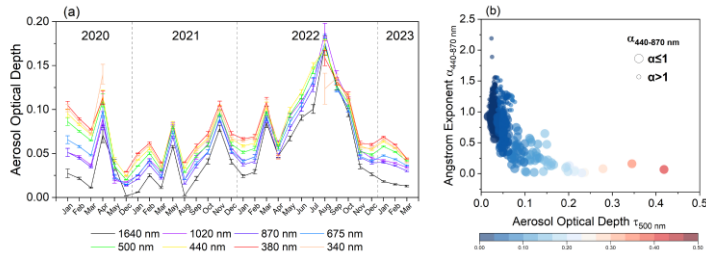
155

156 **Figure 2 (a) Monthly variation of mean aerosol optical depth at different wavelengths measured over**
157 **Zhongshan Station in Antarctica from 2020 to 2023. (b) Relationship between AOD$_{500\ nm}$ and AE$_{440\text{-}870\ nm}$ over**
158 **Zhongshan Station from 2020 to 2023.**

159 **Table 1 Annual mean and standard deviation of aerosol optical depth at different wavelengths and Angstrom**
160 **Exponent at 440-870 nm at Zhongshan Station from 2020 to 2023.**

161

	2020	2021	2022	2023
AOD$_{1640\ nm}$	0.028±0.102	0.026±0.079	0.050±0.141	0.016±0.036
AOD$_{1020\ nm}$	0.049±0.095	0.045±0.073	0.067±0.131	0.040±0.034
AOD$_{870\ nm}$	0.047±0.093	0.039±0.070	0.060±0.126	0.037±0.032
AOD$_{675\ nm}$	0.059±0.091	0.042±0.068	0.063±0.122	0.044±0.031
AOD$_{500\ nm}$	0.074±0.090	0.051±0.066	0.071±0.117	0.053±0.031
AOD$_{440\ nm}$	0.081±0.089	0.057±0.065	0.077±0.116	0.057±0.031
AOD$_{380\ nm}$	0.089±0.091	0.063±0.065	0.077±0.117	0.061±0.032
AOD$_{340\ nm}$	0.088±0.095	0.059±0.064	0.073±0.118	0.058±0.032
AE$_{440\text{-}870\ nm}$	1.134±0.411	0.953±0.338	0.883±0.374	0.753±0.206

162

163 **3.2 Seasonal and Monthly Variations in AOD and Ångström Exponent**

164 The seasonal variation of AOD$_{500\ nm}$ and AE$_{440\text{-}870\ nm}$ over Zhongshan Station suggests the median AOD$_{500}$

165 $_{nm}$ values are lower in spring (0.033), summer (0.036), and autumn (0.045), but higher in winter (0.115),

166 while the AE$_{440\text{-}870\ nm}$ values are 0.908, 1.010, 1.036, and 0.381, respectively (Fig. 4a). The frequency

> 删除了: 3a

167 histograms show that the highest frequency range of AOD$_{500\ nm}$ is 0.02 to 0.04 in spring, summer, and

168 autumn, while 0.08 to 0.12 in winter (Fig. S2). The normal fitting curves of the frequency histograms of

AE$_{440-870 \text{ nm}}$ indicate that the peak in winter is in the low-value range (0.3~0.4), while the peaks in spring, summer, and autumn are in the high-value range (1.0~1.2). To investigate the seasonal differences in AOD$_{500 \text{ nm}}$ and AE$_{440-870 \text{ nm}}$, it is essential to understand the sources of air masses influencing aerosols at Zhongshan Station. Therefore, we calculate the 168h backward trajectory once every 24h from January 2020 to December 2022, with the starting height of 500 m and the starting time of 18:00 (13:00 local time at Zhongshan Station), and clustered by season (Fig. 3). We observed that the proportion of air masses originating from the surrounding waters (red clusters) and the ice edge margin of ice sheet (blue clusters) ranges from 50% to 80%, dominating throughout the year. These air masses are likely the primary sources of local or natural aerosols in Antarctica. In contrast, the proportion of distant origin (yellow and green clusters) is approximately 20%, but it significantly increases in autumn, reaching around 45%. These air masses are associated with long-range transported aerosols. Therefore, the seasonal differences in AOD$_{500 \text{ nm}}$ and AE$_{440-870 \text{ nm}}$ at Zhongshan Station are largely attributed to variations in the types and concentrations of local aerosols.

The seasonal variations in AOD and AE are consistent with previous findings on sea salt aerosol concentrations, although the mechanism behind this seasonal variation is multifaceted. Wang and Huang et al. have indicated that higher winter wind speeds at Zhongshan Station can elevate marine source aerosol concentrations, primarily composed of sea salt, potentially explaining the winter peak in sea salt concentration (Hong et al., 2009; Huang et al., 2005). However, Hall and Wolff propose that the high sea salt load correlates more with moderate wind speeds and shifts in wind direction, rather than high wind speeds, with concentrated brine on freshly formed ice surfaces acting as a source of winter sea salt (Hall and Wolff, 1998). Moreover, blowing snow over sea ice generates aerosols primarily made of sea salt, contributing to the winter peak in sea salt aerosols (Frey et al., 2020). In summer, lower sea salt concentrations lead to lower background levels of AOD, but the effect of enhanced marine biogenic emissions on AOD may increase. In the marine boundary layer over the eastern Southern Ocean sector, $nssSO_4^{2-}$ and MSA contribute approximately 40% of the total mass of fine aerosols (particle size < 0.56 μm) (Xu et al., 2021). Xu et al. reported the annual mean concentrations of $nssSO_4^{2-}$ and MSA at Zhongshan Station were 0-79 $ng\,m^{-3}$ and 19-41 $ng\,m^{-3}$, respectively, with the maximum concentrations were observed in summer (Xu et al., 2019). This increase in summer concentrations is

删除了:

attributed to enhanced solar radiation, phytoplankton blooms in the polynyas releasing DMS (Zhang et al., 2015), and the DMS in the atmosphere is oxidized by radicals such as O_3 (significant at high latitudes), OH, and BrO in the gas phase (Boucher et al., 2003), resulting in elevated concentrations of MSA and $nssSO_4^{2-}$. The positive correlation between mean surface chlorophyll and AOD in the Southern Ocean confirmed the contribution of DMS flux to aerosol load during summer (Gabric et al., 2005).

The monthly variations in $AOD_{500\ nm}$ and $AE_{440-870\ nm}$ at Zhongshan Station suggest an opposite trend, with the mean values of $AOD_{500\ nm}$ peaking in July and $AE_{440-870\ nm}$ reaching its lowest in June (Fig. 4b). Median $AOD_{500\ nm}$ values increase slightly from January to February, followed by a decrease in March and increase continuously from March to August, reach the maximum value, then gradually decrease, and reach the minimum in November and December. The percentages of $AE_{440-870\ nm} > 1.0$ and $AE_{440-8870\ nm} < 1.0$ represent the proportion of the monthly occurrence frequency of fine and coarse mode particles (Fig. 4c). The monthly mean and median $AOD_{500\ nm}$ values are consistent with the proportion of coarse mode particles ($AE_{440-870\ nm} > 1.0$), suggesting that the variation characteristics of $AOD_{500\ nm}$ at Zhongshan Station are primarily influenced by coarse mode particles. Given that Zhongshan Station is located in the coastal area of Antarctica, it is suspected that these coarse particles may be sea salt aerosols.
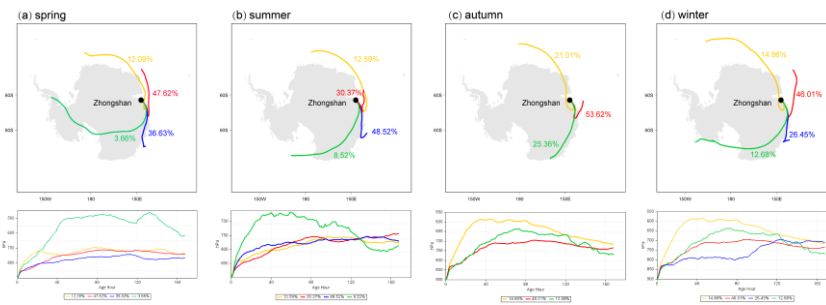
Figure 3 Clusters of air mass backward trajectories in (a) spring, (b) summer, (c) autumn and (d) winter at Zhongshan Station from 2020 to2022.

220
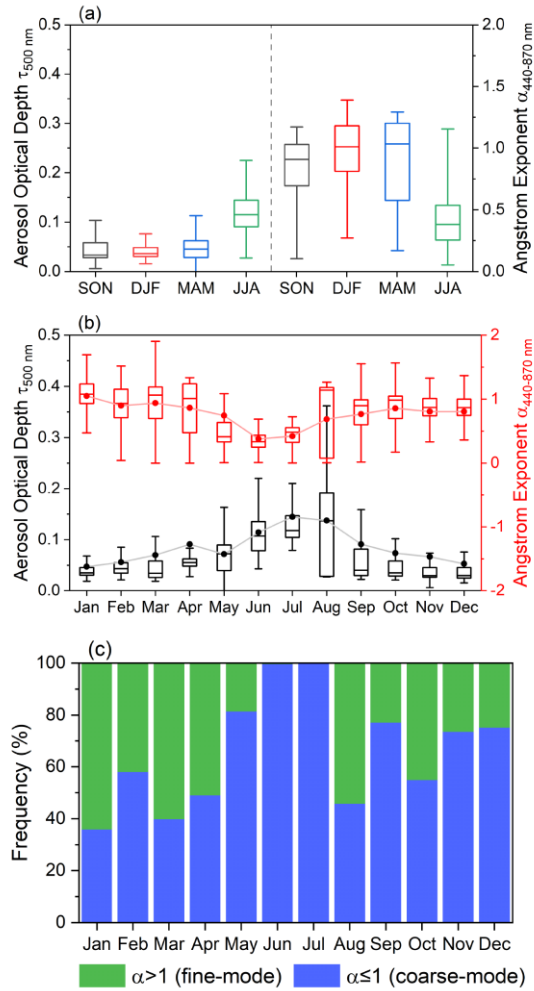
Figure 4 (a) Seasonal variation of aerosol optical depth at 500 nm and Angstrom exponent at 440-870 nm over Zhongshan Station. For each monthly box, the central line indicates the median; and the bottom and top edges of the box indicate the 25th and 75th percentiles, respectively. (b) Variations in monthly AOD$_{500\,nm}$ and AE$_{440-870\,nm}$ at Zhongshan Station. For each monthly box, the central line indicates the median; the dot represents the mean; and the bottom and top edges of the box indicate the 25th and 75th percentiles, respectively. (c) Monthly percentages of Ångström exponent >1.0 (green) and Ångström exponent ≤ 1.0 (blue) at Zhongshan Station from 2020 to 2023.

Additionally, we used a graphical method proposed by Gobbi et al (Gobbi et al., 2007), which is based on Mie calculation and correlates Ångström exponent (α) and Ångström exponent spectral difference ($\delta\alpha$) with fine mode aerosol effective radius (R_{eff}) and fine mode fraction to investigate the aerosol

删除了: 3

modification processes at Zhongshan Station in different seasons. Fig. 5 presents a schematic diagram of

the classification of aerosol types using the α and $\delta\alpha$ functions of a dual-mode, lognormal distribution

with refractive index= $1.4 - 0.001i$ as reference. It is known from Jurányi and Weller' research that the

refractive index of Antarctic coastal aerosol is about 1.4, so it seems reasonable to use this reference

(Jurányi and Weller, 2019). We utilized AOD_{440nm}, AOD_{675nm}, and AOD_{870nm} to calculate $\alpha_{440-675nm}$,

$\alpha_{440-870nm}$, and $a_{675-870nm}$, and then get the $\delta\alpha = \alpha_{440-675nm} - a_{675-870nm}$. The negative values of

$\delta\alpha$ indicate the dominance of fine mode aerosol, while positive values indicate the effect of two separate

particle modes (Kaufman, 1993). The solid black line represents the size of fine mode particles (R_{eff}),

and the dashed blue line represents the proportion of the contribution of fine mode particles to AOD (η).

In Fig. 5, increasing $AOD_{675\,nm}$ is associated with the declining η (spring and winter) and increasing

R_{eff} (summer and autumn). This indicates that higher aerosol loads in spring and winter are attributed

to increased coarse-mode particle fractions, whereas in summer and autumn are primarily associated with

the increase of fine-mode particle size. Previous studies have indicated that sea salt dominates winter

aerosols in the coastal areas of Antarctica (Hall and Wolff, 1998; Weller et al., 2008), and Xu et al

observed that the highest mean concentration of sea salt in September at Zhongshan Station, these can

explain the $\delta\alpha$ values are mainly positive in spring and winter, and η is concentrated within the range

of less than 50% (Xu et al., 2019). In summer and autumn, apart from common sea salt aerosols ($\delta\alpha > 0$,

$\eta < 50$), the high AOD is mainly related to the particle growth such as hygroscopic growth or

condensation of fine mode aerosols ($R_{eff}: 0.10\mu m \sim 0.20\mu m$). This may be linked to the atmospheric

oxidation of (DMS) emitted by biological sources in coastal regions, or the aging process of aerosols

originating from other sources, as the rate of new particle formation and particulate matter growth in

summer is much greater than in winter in the Antarctica (Davison et al., 1996; Lachlan-Cope et al., 2020;

Weller et al., 2015).
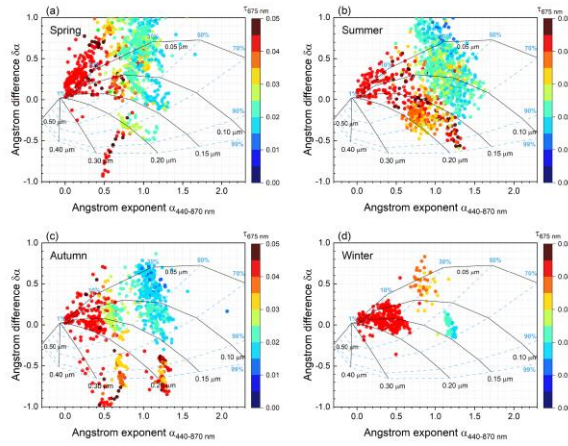
258

259 **Figure 5 Ångström exponent difference ($\delta\alpha = \alpha_{440-675\ nm} - \alpha_{675-870\ nm}$) as a function of the $\alpha_{440-870\ nm}$**

260 **and $AOD_{675\ nm}$ (colour scale) during (a) spring, (b) summer, (c) autumn, and (d) winter at Zhongshan Station.**

261 **The black lines indicate the R_{eff} of fine-mode aerosols, while the blue lines correspond to fine-mode fraction**

262 **(η).**

263 **3.3 Relationship between AOD, Ångström Exponent and Meteorological Conditions**

264 In this section, we analyse the diurnal variation characteristics of $AOD_{500\ nm}$ and $AE_{440-870\ nm}$ during

265 summer and explore their correlation with meteorological variables within the planetary boundary layer

266 (PBL), such as wind directions and speeds, temperature, and relative humidity. We calculated the diurnal

267 variations of $AOD_{500\ nm}$ and $AE_{440-870\ nm}$ based on observations collected at Zhongshan Station during

268 summer (December-February, 2020-2023), with each hourly mean containing at least one thousand

269 individual observations (Fig. 6). The mean $AOD_{500\ nm}$ exhibited an increase from 5:00 to 14:00 (local

270 time of Zhongshan Station), reaching a maximum value (0.06±0.04), and then decreased. The mean

271 $AE_{440-870\ nm}$ decreased from 5:00 to 12:00, reaching the lowest value (0.85±0.25), and then increased.

272 These results indicate that the highest aerosol load occurs at 14:00, accompanied by a larger aerosol

273 particle size during this period. The diurnal variation of boundary layer height (BLH) is almost consistent

274 with the variation of $AOD_{500\ nm}$, which is inconsistent with the general conclusion that the negative

275 correlation between BLH and particulate matter concentration in the mid-latitudes (Lou et al., 2019;

276 Miao and Liu, 2019). However, a minor decline in BLH is noticeable when the $AOD_{500\ nm}$ value reaches

277 its peak at 14:00. Consequently, we suspect that the weak absorption and low content of Antarctic

aerosols typically do not suffice to form an "aerosol-boundary layer" positive feedback mechanism, but

may contribute to reducing the BLH when AOD is high (Lou et al., 2019; Petäjä et al., 2016).
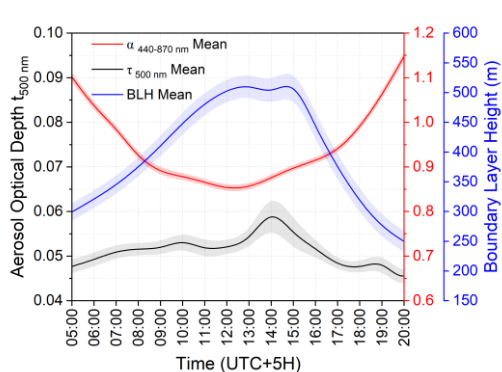
Figure 6 Diurnal variation of AOD$_{500 nm}$ and AE$_{440-870 nm}$ at Zhongshan Station. The black line indicates the mean of AOD$_{500 nm}$; the red line represents the mean of AE$_{440-870 nm}$; the blue line represents the mean of BLH. The shadow represents the standard deviation of the mean.

Moreover, the 2-minute average wind direction at Zhongshan Station mainly comes from the southeast

with the diurnal variation of the 2-minute average wind speeds ranging from 2 to 9 m s^{-1}. There is a

noticeable decline in wind speeds between 5:00 and 14:00, followed by a gradual increase thereafter (Fig.

7). Given that the CE318-T is positioned westward of the main Zhongshan Station building, the eastward

winds may carry emissions originating from western stations such as Zhongshan and Progress Station.

The relationship between the diurnal variation of AOD$_{500 nm}$ and wind speed is more obvious: AOD$_{500 nm}$

exhibits a decline (increase) concurrent with increasing (decreasing) wind speeds. This correlation stems

from the fact that higher wind speeds facilitate the dispersion of pollutants, leading to a reduction in

AOD, and vice versa (Coccia, 2021; Liu et al., 2020; Wang et al., 2022).

302
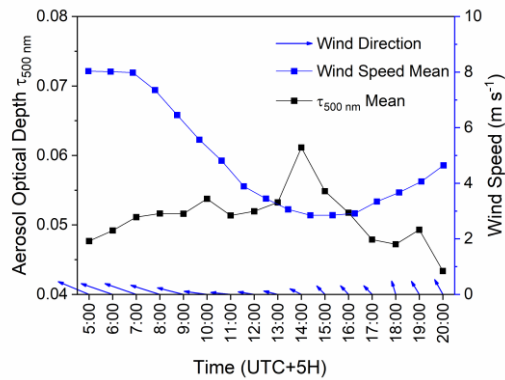
Figure 7. Diurnal variations of 2-minute average wind direction, 2-minute average speed, and AOD$_{500\ nm}$ in

304 **summer at Zhongshan Station.**

305 The influence of temperature and relative humidity on aerosol parameters is relatively complex.

306 Temperature affects aerosol particle concentration by influencing the air convection and influencing the

307 formation and optical properties of secondary by controlling chemical transformation (Han et al., 2007;

308 Li et al., 2020). Relative humidity affects the chemical composition, size distribution, and optical

309 properties of aerosol particles by affecting their aqueous-phase reactions and gas-particle partitioning

310 (Altieri et al., 2008; Ding et al., 2021; Hennigan et al., 2008; Sun et al., 2013). The diurnal variations of

311 AOD$_{500\ nm}$, temperature, and relative humidity in summer at Zhongshan Station show that AOD$_{500\ nm}$ is

312 positively correlated with temperature with a correlation coefficient of 0.22, and AOD$_{500\ nm}$ is negatively

313 correlated with relative humidity with a correlation coefficient of -0.59 (Fig. 8). This indicates that rising

314 (declining) temperature and declining (rising) relative humidity during the day may contribute to an

315 increase (declining) in aerosol load. Previous studies have shown a positive correlation between

316 temperature and AOD (Basharat et al., 2023). During the summer at Zhongshan Station, high

317 temperatures may destroy the physical properties of bare rocks and promote the formation and diffusion

318 of particulate matter, thereby increasing the aerosol load (Zhang, 2024). However, there is a study

319 showing that higher temperatures may reduce methane sulfinic acid (MSIA) yield (Cecilia Arsene et al.,

320 1999). Therefore, the effect of temperature on the AOD at Zhongshan Station is complex, resulting in an

321 insignificant positive correlation. The relationship between relative humidity and AOD is inconclusive

322 (Gautam et al., 2022), as high relative humidity may contribute to the increase of aerosol hygroscopic

323 properties leading to an increase in AOD (Meng et al., 2024), or it may contribute to a decrease in AOD

删除了: 6

删除了: and

删除了: 7

327 by reducing dust particles in the air (Zhang, 2024). Therefore, the influence of temperature and relative

328 humidity on AOD may be related to the physicochemical properties of local aerosols and their sourcing

329 and sink processes.

330
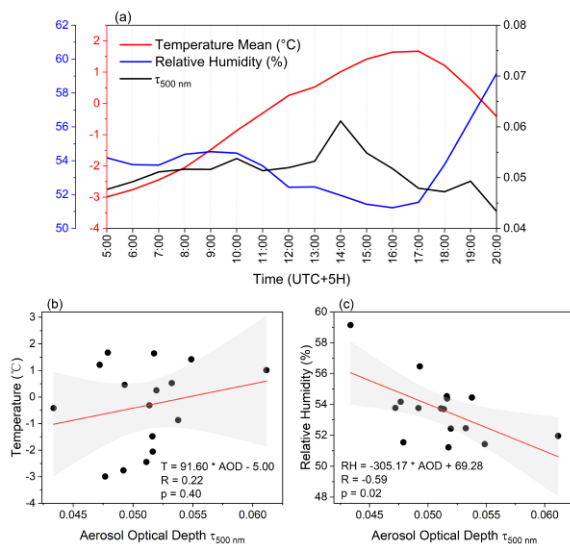
Figure 8 (a) Diurnal variations of AOD$_{500\ nm}$ (black), temperature (red), and relative humidity (blue) in summer at Zhongshan Station; (b) relationship between AOD$_{500\ nm}$ and temperature; and (c) relationship between AOD$_{500\ nm}$ and relative humidity. The red line indicates the regression line obtained by fitting a linear regression, and the grey bands indicate the confidence intervals for the linear regression.

335 **4 Discussion**

336 **4.1 Potential effects of aerosol sources on AOD levels**

337 Besides meteorological conditions, aerosol sources may also influence the diurnal variation

338 characteristics of AOD. We classified days with mean AOD below the 5th percentile as low AOD day

339 and those above the 95th percentile as high AOD day (Fig. S3 and Table S1). Using the HYSPLIT

340 backward trajectory model, we found that air masses on high AOD days primarily originated from the

341 ocean, whereas those on low AOD days mostly came from the interior of Antarctica (Fig. S4). The

342 altitudes of the backward trajectories show that during low AOD days, the air mass originating from the

343 ocean usually starts at a lower altitude (<1000 m), rises to a higher altitude (~2000 m) and then descends

344 to Zhongshan Station (2020-05-15 and 2020-12-25), while the air mass originating from the interior of

346 Antarctica usually starts at a higher altitude (~3000 m) and then descends to Zhongshan Station. This

347 indicates that particles from the Antarctic plateau or the free troposphere above the Antarctic interior are

348 transported to Zhongshan Station by katabatic winds. Researches show that the katabatic winds driven

349 by latent cooling occurring in the high-wind East Antarctic can rush the dense air from the interior plateau

350 to the coast (Simmons et al., 2021; Yu et al., 2020). Combined with the AE values, we can find that the

351 AE values of low AOD days are usually greater than 1, indicating the small particle size, thus, we suspect

352 that these fine particles may be $nssSO_4^{2-}$ from the Antarctic interior (Pei et al., 2021). In contrast, in

353 high AOD days, the air mass all originates in the ocean and usually starts at a lower altitude. The AE

354 values corresponding to high AOD moment on high AOD days are extremely low (<0.5), indicating that

355 the particle size is large, thus, we suspect that these aerosols may consist of coarse sea salt particles.

356 **4.2 Potential effects of aerosol particles on cloud and radiative forcing**

357 The optical properties of aerosols play a crucial role in their impact on radiative forcing, cloud formation,

358 and local climate. In our analysis of the variations in AOD and AE, we provided insights into the aerosol

359 loading, particle sizes, and possible formation and growth mechanisms in the atmosphere over

360 Zhongshan Station. During winter and spring, coarse mode particles are predominantly derived from sea

361 salt. Studies have shown that aerosols larger than 0.13 μm in the marine boundary layer contain sea salt,

362 contributing to most of the aerosol scattering and inducing cooling effects (Murphy et al., 1998).

363 Additionally, the size and inhomogeneity of sea salt particles are often associated with relative humidity.

364 Compared to remote oceans, the low relative humidity in coastal Antarctica may introduce more

365 inhomogeneous sea salt particles, resulting in up to a 12% change in direct radiative forcing due to

366 inhomogeneity (Wang et al., 2019).

367 However, we are particularly interested in the behaviour of aerosol particles during summer since solar

368 radiation is limited in winter. In summer and autumn, the increase in fine mode particles in closely related

369 to the release of biogenic aerosols, such as DMS, emitted by phytoplankton in the marginal ice zone.

370 When particles grow to a size suitable for cloud condensation nuclei or ice nucleating particles, they can

371 affect the formation of low-level mixed-phase clouds in coastal areas, contributing to the formation of

372 low-level ice clouds. At the same time, the increased number density of cloud droplets enhances cloud

373 reflectivity, resulting in negative radiative forcing (Satheesh and Krishna Moorthy, 2005). A recent study

374   revealed that in the shallow mixed-phase clouds over Antarctica, the concentrations of cloud-relevant

375   aerosol particles match the concentrations of ice crystals and cloud droplets (Radenz et al., 2024). the

376   number of particles plays a crucial role in cloud growth. Increasing particle concentration results in a

377   higher abundance of liquid droplets and ice crystals within clouds, which can impact cloud lifespan and

378   potentially influence local weather and climate. Therefore, continuous monitoring of aerosol optical

379   properties in coastal Antarctica is vital to improve our comprehension of aerosol radiative forcing

380   variations caused by changes in aerosol loading and particle size.

381   **5 Summary**

382   This study analysed the AOD and AE variations retrieved from CE318-T sun photometer data spanning

383   from January 2020 to April 2023 at Zhongshan Station in Antarctica. The main conclusions we draw are

384   as follows:

385   At Zhongshan Station, AOD varied from 0.00 to 0.20. Fine mode particles were predominantly found in

386   the lower AOD range, while higher AOD values were mainly attributed to coarse mode particles.

387   Seasonally, AOD exhibited a pattern of lower values in summer and higher values in winter, and the AE

388   displayed an opposite trend. The increases in AOD during summer and autumn may be linked to particle

389   growth, whereas the increases during spring and winter are associated with a decline in the fraction of

390   fine mode particles.

391   Low aerosol load over Zhongshan Station was not enough to form an "aerosol-boundary layer" positive

392   feedback mechanism, but the slight decrease in BLH may be related to AOD diurnal peak at 14:00.

393   Moreover, high (low) wind speeds facilitated pollutant dispersion (accumulation), leading to reduced

394   (increased) AOD. A weak positive correlation was noted between temperature and AOD (R = 0.22, p =

395   0.40), and a negative correlation between relative humidity and AOD (R = -0.59, p = 0.02). The

396   mechanisms underlying temperature and humidity's influence on aerosols remain unclear, possibly

397   linked to local aerosol properties at Zhongshan Station. In addition, we discuss the influence of aerosol

398   sources on AOD. The backward trajectories show that the air masses on high AOD days come from the

399   ocean, and the low AE values indicate that the particle size is larger, we speculate that the main

400   composition of the aerosols is sea salt. The air masses on the low AOD days mainly come from the

401 interior of Antarctica, and the high AE values indicate that the particle size is small. We speculate that

402 the katabatic winds rush the air from the Antarctic plateau to Zhongshan Station.

403 **Data availability**

404 The data included in this study can be accessed via https://zenodo.org/records/10983098. Boundary layer

405 height data downloaded from ECMWF ERA5 (https://www.ecmwf.int/en/forecasts/dataset/ecmwf-

406 reanalysis-v5). Backward trajectory of air mass and the meteorological data are obtained from NOAA

407 Air Resources Laboratory (https://www.ready.noaa.gov/HYSPLIT_traj.php).

删除了:

408 **Author contributions**

409 The paper is a result of the lead author's research work under the supervision of MD, LZ, YS. ZZ and

410 YZ provided constructive comments. LZ assisted in the respond of the review comments. MD, QW and

411 BT provided experimental data. ZL provided aerial photos of Zhongshan Station. LC wrote the first draft

412 of the paper with the help and support of all the authors. HC provided guidance for the manuscript

413 revisions.

414 **Competing interests**

415 The contact author has declared that none of the authors has any competing interests.

416 **Acknowledgments**

417 Funding for this study was provided by the National Natural Science Foundation of China (42122047),

418 the National Key Research and Development Program of China (2021YFC2802504), and the Basic

419 Research Fund of the Chinese Academy of Meteorological Science (2023Z015&2023Z025).

420 **Reference**

421 Alghoul, M., Khamies, H., Assadeg, J., Yahya, M., Alfegi, E., and Sopian, K.:
422 Impact of Aerosol Optical Depth on Solar Radiation Budget, in: Proceedings of the 3rd
423 World Scientific and Engineering Academy and Society Int., Conference on renewable
424 energy sources, 2009.

426   Altieri, K. E., Seitzinger, S. P., Carlton, A. G., Turpin, B. J., Klein, G. C., and
427   Marshall, A. G.: Oligomers formed through in-cloud methylglyoxal reactions:
428   Chemical composition, properties, and mechanisms investigated by ultra-high
429   resolution FT-ICR mass spectrometry, Atmospheric Environment, 42, 1476–1490,
430   https://doi.org/10.1016/j.atmosenv.2007.11.015, 2008.

431   Barreto, Á., Cuevas, E., Granados-Muñoz, M.-J., Alados-Arboledas, L., Romero,
432   P. M., Gröbner, J., Kouremeti, N., Almansa, A. F., Stone, T., Toledano, C., Román, R.,
433   Sorokin, M., Holben, B., Canini, M., and Yela, M.: The new sun-sky-lunar Cimel
434   CE318-T multiband photometer - a comprehensive performance evaluation,
435   Atmospheric Measurement Techniques, 9, 631–654, https://doi.org/10.5194/amt-9-
436   631-2016, 2016.

437   Basharat, U., Tariq, S., Chaudhry, M. N., Khan, M., Bonah Agyekum, E., Fendzi
438   Mbasso, W., and Kamel, S.: Seasonal correlation of aerosols with soil moisture,
439   evapotranspiration, and vegetation over Pakistan using remote sensing, Heliyon, 9,
440   e20635, https://doi.org/10.1016/j.heliyon.2023.e20635, 2023.

441   Boucher, O., Moulin, C., Belviso, S., Aumont, O., Bopp, L., Cosme, E., von
442   Kuhlmann, R., Lawrence, M. G., Pham, M., Reddy, M. S., Sciare, J., and Venkataraman,
443   C.: DMS atmospheric concentrations and sulphate aerosol indirect radiative forcing: a
444   sensitivity study to the DMS source representation and oxidation, Atmospheric
445   Chemistry and Physics, 3, 49–65, https://doi.org/10.5194/acp-3-49-2003, 2003.

446   Cecilia Arsene, Barnes, I., and Becker, K. H.: FT-IR product study of the photo-
447   oxidation of dimethyl sulfide: Temperature and O2 partial pressure dependence,
448   Physical   Chemistry   Chemical   Physics,   1,   5463–5470,
449   https://doi.org/10.1039/A907211J, 1999.

450   Che, H., Xia, X., Zhao, H., Li, L., Gui, K., Zheng, Y., Song, J., Qi, B., Zhu, J.,
451   Miao, Y., Wang, Y., Wang, Z., Wang, H., Dubovik, O., Holben, B., Chen, H., Shi, G.,
452   and Zhang, X.: Aerosol optical and radiative properties and their environmental effects
453   in   China: A   review,   Earth-Science   Reviews,   248,   104634,
454   https://doi.org/10.1016/j.earscirev.2023.104634, 2024.

455   Coccia, M.: How do low wind speeds and high levels of air pollution support the
456   spread   of   COVID-19?,   Atmos   Pollut   Res,   12,   437–445,
457   https://doi.org/10.1016/j.apr.2020.10.002, 2021.

458   Davison, B., O'dowd, C., Hewitt, C. N., Smith, M. H., Harrison, R. M., Peel, D.
459   A., Wolf, E., Mulvaney, R., Schwikowski, M., and Baltenspergert, U.: Dimethyl sulfide
460   and its oxidation products in the atmosphere of the Atlantic and Southern Oceans,
461   Atmospheric   Environment,   30,   1895–1906,   https://doi.org/10.1016/1352-
462   2310(95)00428-9, 1996.

463 Ding, J., Dai, Q., Zhang, Y., Xu, J., Huangfu, Y., and Feng, Y.: Air humidity affects
464 secondary aerosol formation in different pathways, Science of The Total Environment,
465 759, 143540, https://doi.org/10.1016/j.scitotenv.2020.143540, 2021.

466 Ding, M., Zou, X., Sun, Q., Yang, D., Zhang, W., Bian, L., Lu, C., Allison, I., Heil,
467 P., and Xiao, C.: The PANDA automatic weather station network between the coast and
468 Dome A, East Antarctica, Earth System Science Data, 14, 5019–5035,
469 https://doi.org/10.5194/essd-14-5019-2022, 2022.

470 Frey, M. M., Norris, S. J., Brooks, I. M., Anderson, P. S., Nishimura, K., Yang, X.,
471 Jones, A. E., Nerentorp Mastromonaco, M. G., Jones, D. H., and Wolff, E. W.: First
472 direct observation of sea salt aerosol production from blowing snow above sea ice,
473 Atmospheric Chemistry and Physics, 20, 2549–2578, https://doi.org/10.5194/acp-20-
474 2549-2020, 2020.

475 Gabric, A. J., Shephard, J. M., Knight, J. M., Jones, G., and Trevena, A. J.:
476 Correlations between the satellite-derived seasonal cycles of phytoplankton biomass
477 and aerosol optical depth in the Southern Ocean: Evidence for the influence of sea ice,
478 Global Biogeochemical Cycles, 19, https://doi.org/10.1029/2005GB002546, 2005.

479 Gadhavi, H. and Achuthan, J.: Aerosol characteristics and aerosol radiative forcing
480 over Maitri, Antarctica, Current Sciecne, 86, 296, 2004.

481 Gautam, S., Elizabeth, J., Gautam, A. S., Singh, K., and Abhilash, P.: Impact
482 Assessment of Aerosol Optical Depth on Rainfall in Indian Rural Areas, Aerosol
483 Science and Engineering, 6, 186–196, https://doi.org/10.1007/s41810-022-00134-9,
484 2022.

485 Gobbi, G. P., Kaufman, Y. J., Koren, I., and Eck, T. F.: Classification of aerosol
486 properties derived from AERONET direct sun data, Atmospheric Chemistry and
487 Physics, 7, 453–458, https://doi.org/10.5194/acp-7-453-2007, 2007.

488 Hall, J. S. and Wolff, E. W.: Causes of seasonal and daily variations in aerosol sea-
489 salt concentrations at a coastal Antarctic station, Atmospheric Environment, 32, 3669–
490 3677, https://doi.org/10.1016/S1352-2310(98)00090-9, 1998.

491 Han, D., Liu, W., Zhang, Y., Lu, Y., Liu, J., and Zhao, N.: Influence of temperature
492 and relative humidity upon aerosol mass concentrations vertical distributions, Journal
493 of University of Chinese Academy of Sciences, 24, 619,
494 https://doi.org/10.7523/j.issn.2095-6134.2007.5.011, 2007.

495 Harder, S., Warren, S. G., and Charlson, R. J.: Sulfate in air and snow at the South
496 Pole: Implications for transport and deposition at sites with low snow accumulation,
497 Journal of Geophysical Research: Atmospheres, 105, 22825–22832,
498 https://doi.org/10.1029/2000JD900351, 2000.

499   Hennigan, C. J., Bergin, M. H., Dibb, J. E., and Weber, R. J.: Enhanced secondary
500 organic aerosol formation due to water uptake by fine particles, Geophysical Research
501 Letters, 35, https://doi.org/10.1029/2008GL035046, 2008.

502   Hong, J., Chen, L., and Yang, X.: Characteristics of the aerosols in Zhongshan
503 Station, Antarctica (in Chinese), Chinese Journal of Polar Research, 21, 1, 2009.

504   Huang, Z., Ji, W., Yang, X., Huang, R., Tang, R., Yu, T., and Zhang, G.: The
505 chemical composition of marine aerosol over Zhongshan Station in Antarctica and its
506 sources discrimination in 1998 (in Chinese), Acta Oceanologica Sinica, 27, 59–66,
507 2005.

508   Jurányi, Z. and Weller, R.: One year of aerosol refractive index measurement from
509 a coastal Antarctic site, Atmospheric Chemistry and Physics, 19, 14417–14430,
510 https://doi.org/10.5194/acp-19-14417-2019, 2019.

511   Kamra, V. P., Devendraa Siingh, A. K.: Antarctic Aerosols and Climate:
512 Measurements at a Coastal Antarctic Station, in: Climate Variability of Southern High
513 Latitude Regions, CRC Press, 2022.

514   Kang, S., Zhang, Y., Qian, Y., and Wang, H.: A review of black carbon in snow
515 and ice and its impact on the cryosphere, Earth-Science Reviews, 210, 103346,
516 https://doi.org/10.1016/j.earscirev.2020.103346, 2020.

517   Kannemadugu, H. B. S., Sudhakaran Syamala, P., Taori, A., Bothale, R. V., and
518 Chauhan, P.: Atmospheric aerosol optical properties and trends over Antarctica using
519 in-situ measurements and MERRA-2 aerosol products, Polar Science, 38, 101011,
520 https://doi.org/10.1016/j.polar.2023.101011, 2023.

521   Kaufman, Y. J.: Aerosol optical thickness and atmospheric path radiance, Journal
522 of Geophysical Research: Atmospheres, 98, 2677–2692,
523 https://doi.org/10.1029/92JD02427, 1993.

524   Lachlan-Cope, T., Beddows, D. C. S., Brough, N., Jones, A. E., Harrison, R. M.,
525 Lupi, A., Yoon, Y. J., Virkkula, A., and Dall'Osto, M.: On the annual variability of
526 Antarctic aerosol size distributions at Halley Research Station, Atmospheric Chemistry
527 and Physics, 20, 4461–4476, https://doi.org/10.5194/acp-20-4461-2020, 2020.

528   Li, J., Wang, W., Li, K., Zhang, W., Peng, C., Zhou, L., Shi, B., Chen, Y., Liu, M.,
529 Li, H., and Ge, M.: Temperature effects on optical properties and chemical composition
530 of secondary organic aerosol derived from n-dodecane, Atmospheric Chemistry and
531 Physics, 20, 8123–8137, https://doi.org/10.5194/acp-20-8123-2020, 2020.

532   Li, J., Carlson, B. E., Yung, Y. L., Lv, D., Hansen, J., Penner, J. E., Liao, H.,
533 Ramaswamy, V., Kahn, R. A., Zhang, P., Dubovik, O., Ding, A., Lacis, A. A., Zhang,

534 L., and Dong, Y.: Scattering and absorbing aerosols in the climate system, Nat Rev
535 Earth Environ, 3, 363–379, https://doi.org/10.1038/s43017-022-00296-7, 2022.

536 Liu, Y., Zhou, Y., and Lu, J.: Exploring the relationship between air pollution and
537 meteorological conditions in China under environmental governance, Sci Rep, 10,
538 14518, https://doi.org/10.1038/s41598-020-71338-7, 2020.

539 Lou, M., Guo, J., Wang, L., Xu, H., Chen, D., Miao, Y., Lv, Y., Li, Y., Guo, X., Ma,
540 S., and Li, J.: On the Relationship Between Aerosol and Boundary Layer Height in
541 Summer in China Under Different Thermodynamic Conditions, Earth and Space
542 Science, 6, 887–901, https://doi.org/10.1029/2019EA000620, 2019.

543 Meng, H., Bai, G., and Wang, L.: Analysis of the spatial and temporal distribution
544 characteristics of AOD in typical industrial cities in northwest China and the influence
545 of meteorological factors, Atmospheric Pollution Research, 15, 101957,
546 https://doi.org/10.1016/j.apr.2023.101957, 2024.

547 Miao, Y. and Liu, S.: Linkages between aerosol pollution and planetary boundary
548 layer structure in China, Science of The Total Environment, 650, 288–296,
549 https://doi.org/10.1016/j.scitotenv.2018.09.032, 2019.

550 Murphy, D. M., Anderson, J. R., Quinn, P. K., McInnes, L. M., Brechtel, F. J.,
551 Kreidenweis, S. M., Middlebrook, A. M., Pósfai, M., Thomson, D. S., and Buseck, P.
552 R.: Influence of sea-salt on aerosol radiative properties in the Southern Ocean marine
553 boundary layer, Nature, 392, 62–65, https://doi.org/10.1038/32138, 1998.

554 Pei, Q., Saikawa, E., Kaspari, S., Widory, D., Zhao, C., Wu, G., Loewen, M., Wan,
555 X., Kang, S., Wang, X., Zhang, Y.-L., and Cong, Z.: Sulfur aerosols in the Arctic,
556 Antarctic, and Tibetan Plateau: Current knowledge and future perspectives, Earth-
557 Science Reviews, 220, 103753, https://doi.org/10.1016/j.earscirev.2021.103753, 2021.

558 Petäjä, T., Järvi, L., Kerminen, V.-M., Ding, A. J., Sun, J. N., Nie, W., Kujansuu,
559 J., Virkkula, A., Yang, X., Fu, C. B., Zilitinkevich, S., and Kulmala, M.: Enhanced air
560 pollution via aerosol-boundary layer feedback in China, Sci Rep, 6, 18998,
561 https://doi.org/10.1038/srep18998, 2016.

562 Radenz, M., Engelmann, R., Henning, S., Schmithüsen, H., Baars, H., Frey, M. M.,
563 Weller, R., Bühl, J., Jimenez, C., Roschke, J., Muser, L. O., Wullenweber, N.,
564 Zeppenfeld, S., Griesche, H., Wandinger, U., and Seifert, P.: Ground-based Remote
565 Sensing of Aerosol, Clouds, Dynamics, and Precipitation in Antarctica —First results
566 from the one-year COALA campaign at Neumayer Station III in 2023,
567 https://doi.org/10.1175/BAMS-D-22-0285.1, 2024.

568 Satheesh, S. K. and Krishna Moorthy, K.: Radiative effects of natural aerosols: A
569 review, Atmospheric Environment, 39, 2089–2110,

570   https://doi.org/10.1016/j.atmosenv.2004.12.029, 2005.

571   Schuster, G. L., Dubovik, O., and Holben, B. N.: Angstrom exponent and bimodal
572   aerosol size distributions, Journal of Geophysical Research: Atmospheres, 111,
573   https://doi.org/10.1029/2005JD006328, 2006.

574   Shaw, G. E.: Considerations on the origin and properties of the Antarctic aerosol,
575   Reviews of Geophysics, 17, 1983–1998, https://doi.org/10.1029/RG017i008p01983,
576   1979.

577   Simmons, J. B., Humphries, R. S., Wilson, S. R., Chambers, S. D., Williams, A.
578   G., Griffiths, A. D., McRobert, I. M., Ward, J. P., Keywood, M. D., and Gribben, S.:
579   Summer aerosol measurements over the East Antarctic seasonal ice zone, Atmospheric
580   Chemistry and Physics, 21, 9497–9513, https://doi.org/10.5194/acp-21-9497-2021,
581   2021.

582   Su, Y., Han, Y., Luo, H., Zhang, Y., Shao, S., and Xie, X.: Physical-Optical
583   Properties of Marine Aerosols over the South China Sea: Shipboard Measurements and
584   MERRA-2 Reanalysis, Remote Sensing, 14, 2453, https://doi.org/10.3390/rs14102453,
585   2022.

586   Sun, Y., Wang, Z., Fu, P., Jiang, Q., Yang, T., Li, J., and Ge, X.: The impact of
587   relative humidity on aerosol composition and evolution processes during wintertime in
588   Beijing,   China,   Atmospheric   Environment,   77,   927–934,
589   https://doi.org/10.1016/j.atmosenv.2013.06.019, 2013.

590   Thakur, R.: Trace elemental variability in aerosols near the two Indian Antarctic
591   research stations during austral summer, No. 26, pp 61–74, 2019.

592   Thornhill, G., Collins, W., Olivié, D., Skeie, R. B., Archibald, A., Bauer, S., Checa-
593   Garcia, R., Fiedler, S., Folberth, G., Gjermundsen, A., Horowitz, L., Lamarque, J.-F.,
594   Michou, M., Mulcahy, J., Nabat, P., Naik, V., O'Connor, F. M., Paulot, F., Schulz, M.,
595   Scott, C. E., Séférian, R., Smith, C., Takemura, T., Tilmes, S., Tsigaridis, K., and Weber,
596   J.: Climate-driven chemistry and aerosol feedbacks in CMIP6 Earth system models,
597   Atmos. Chem. Phys., 21, 1105–1126, https://doi.org/10.5194/acp-21-1105-2021, 2021.

598   Tian, B., Ding, M., Putero, D., Li, C., Zhang, D., Tang, J., Zheng, X., Bian, L., and
599   Xiao, C.: Multi-year variation of near-surface ozone at Zhongshan Station, Antarctica,
600   Environ. Res. Lett., 17, 044003, https://doi.org/10.1088/1748-9326/ac583c, 2022.

601   Tomasi, C., Vitale, V., Lupi, A., Di Carmine, C., Campanelli, M., Herber, A.,
602   Treffeisen, R., Stone, R. S., Andrews, E., Sharma, S., Radionov, V., von Hoyningen-
603   Huene, W., Stebel, K., Hansen, G. H., Myhre, C. L., Wehrli, C., Aaltonen, V.,
604   Lihavainen, H., Virkkula, A., Hillamo, R., Ström, J., Toledano, C., Cachorro, V. E.,
605   Ortiz, P., de Frutos, A. M., Blindheim, S., Frioud, M., Gausa, M., Zielinski, T., Petelski,

606 T., and Yamanouchi, T.: Aerosols in polar regions: A historical overview based on
607 optical depth and in situ observations, Journal of Geophysical Research: Atmospheres,
608 112, https://doi.org/10.1029/2007JD008432, 2007.

609 Tomasi, C., Lupi, A., Mazzola, M., Stone, R. S., Dutton, E. G., Herber, A.,
610 Radionov, V. F., Holben, B. N., Sorokin, M. G., Sakerin, S. M., Terpugova, S. A.,
611 Sobolewski, P. S., Lanconelli, C., Petkov, B. H., Busetto, M., and Vitale, V.: An update
612 on polar aerosol optical properties using POLAR-AOD and other measurements
613 performed during the International Polar Year, Atmospheric Environment, 52, 29–47,
614 https://doi.org/10.1016/j.atmosenv.2012.02.055, 2012.

615 Udisti, R., Dayan, U., Becagli, S., Busetto, M., Frosini, D., Legrand, M., Lucarelli,
616 F., Preunkert, S., Severi, M., Traversi, R., and Vitale, V.: Sea spray aerosol in central
617 Antarctica. Present atmospheric behaviour and implications for paleoclimatic
618 reconstructions, Atmospheric Environment, 52, 109–120,
619 https://doi.org/10.1016/j.atmosenv.2011.10.018, 2012.

620 Virkkula, A., Grythe, H., Backman, J., Petäjä, T., Busetto, M., Lanconelli, C., Lupi,
621 A., Becagli, S., Traversi, R., Severi, M., Vitale, V., Sheridan, P., and Andrews, E.:
622 Aerosol optical properties calculated from size distributions, filter samples and
623 absorption photometer data at Dome C, Antarctica, and their relationships with seasonal
624 cycles of sources, Atmospheric Chemistry and Physics, 22, 5033–5069,
625 https://doi.org/10.5194/acp-22-5033-2022, 2022.

626 Walters, W. W., Michalski, G., Böhlke, J. K., Alexander, B., Savarino, J., and
627 Thiemens, M. H.: Assessing the Seasonal Dynamics of Nitrate and Sulfate Aerosols at
628 the South Pole Utilizing Stable Isotopes, Journal of Geophysical Research:
629 Atmospheres, 124, 8161–8177, https://doi.org/10.1029/2019JD030517, 2019.

630 Wang, X., Chen, L., Guo, K., and Liu, B.: Spatio-temporal trajectory evolution
631 and cause analysis of air pollution in Chengdu, China, Journal of the Air & Waste
632 Management Association, 72, 876–894,
633 https://doi.org/10.1080/10962247.2022.2058642, 2022.

634 Wang, Z., Bi, L., Yi, B., and Zhang, X.: How the Inhomogeneity of Wet Sea Salt
635 Aerosols Affects Direct Radiative Forcing, Geophysical Research Letters, 46, 1805–
636 1813, https://doi.org/10.1029/2018GL081193, 2019.

637 Weller, R. and Lampert, A.: Optical properties and sulfate scattering efficiency of
638 boundary layer aerosol at coastal Neumayer Station, Antarctica, Journal of Geophysical
639 Research: Atmospheres, 113, https://doi.org/10.1029/2008JD009962, 2008.

640 Weller, R., Wöltjen, J., Piel, C., Resenberg, R., Wagenbach, D., König-Langlo, G.,
641 and Kriews, M.: Seasonal variability of crustal and marine trace elements in the aerosol
642 at Neumayer station, Antarctica, Tellus B, 60, 742–752, https://doi.org/10.1111/j.1600-

0889.2008.00372.x, 2008.

Weller, R., Schmidt, K., Teinilä, K., and Hillamo, R.: Natural new particle formation at the coastal Antarctic site Neumayer, Atmospheric Chemistry and Physics, 15, 11399–11410, https://doi.org/10.5194/acp-15-11399-2015, 2015.

Xu, G., Chen, L., Zhang, M., Zhang, Y., Wang, J., and Lin, Q.: Year-round records of bulk aerosol composition over the Zhongshan Station, Coastal East Antarctica, Air Qual Atmos Hlth, 12, 271–288, https://doi.org/10.1007/s11869-018-0642-9, 2019.

Xu, G., Chen, L., Xu, T., He, S., and Gao, Y.: Distributions of water-soluble ions in size-aggregated aerosols over the Southern Ocean and coastal Antarctica, Environ. Sci.: Processes Impacts, 23, 1316–1327, https://doi.org/10.1039/D1EM00089F, 2021.

Yan, J., Jung, J., Lin, Q., Zhang, M., Xu, S., and Zhao, S.: Effect of sea ice retreat on marine aerosol emissions in the Southern Ocean, Antarctica, Sci Total Environ, 745, 140773, https://doi.org/10.1016/j.scitotenv.2020.140773, 2020.

Yang, Y., Zhao, C., Wang, Q., Cong, Z., Yang, X., and Fan, H.: Aerosol characteristics at the three poles of the Earth as characterized by Cloud–Aerosol Lidar and Infrared Pathfinder Satellite Observations, Atmospheric Chemistry and Physics, 21, 4849–4868, https://doi.org/10.5194/acp-21-4849-2021, 2021.

Yu, L., Zhong, S., and Sun, B.: The Climatology and Trend of Surface Wind Speed over Antarctica and the Southern Ocean and the Implication to Wind Energy Application, Atmosphere, 11, 108, https://doi.org/10.3390/atmos11010108, 2020.

Zhang, F.: Factors Influencing the Spatio–Temporal Variability of Aerosol Optical Depth over the Arid Region of Northwest China, Atmosphere, 15, 54, https://doi.org/10.3390/atmos15010054, 2024.

Zhang, M., Chen, L., Xu, G., Lin, Q., and Liang, M.: Linking Phytoplankton Activity in Polynyas and Sulfur Aerosols over Zhongshan Station, East Antarctica, Journal of the Atmospheric Sciences, 72, 4629–4642, https://doi.org/10.1175/JAS-D-15-0094.1, 2015.